Southwest Indian Ocean SST Variability: Its Local Effect and Remote Influence on Asian Monsoons*

H. ANNAMALAI, PING LIU, AND SHANG-PING XIE+

International Pacific Research Center, University of Hawaii at Manoa, Honolulu, Hawaii

(Manuscript received 6 July 2004, in final form 1 February 2005)

ABSTRACT

An atmospheric general circulation model (AGCM) is used to examine the role of Indian Ocean sea surface temperature (SST) anomalies in regional climate variability. In particular, the authors focus on the effect of the basinwide warming that occurs during December through May after the mature phase of El Niño. To elucidate the relative importance of local and remote forcing, model solutions were sought for experiments where SST anomalies are inserted in the (i) tropical Indo-Pacific Oceans, (ii) tropical Pacific Ocean, and (iii) tropical Indian Ocean. A 10-member ensemble simulation is carried out for each of the three forcing scenarios.

The model solutions demonstrate that precipitation variations over the southwest Indian Ocean are tied to local SST anomalies and are highly reproducible. Changes in the Indian Ocean–Walker circulation suppress precipitation over the tropical west Pacific–Maritime Continent, contributing to the development of a low-level anticyclone over the Philippine and South China Seas. Our model results indicate that more than 50% of the total precipitation anomalies over the tropical west Pacific–Maritime Continent is forced by remote Indian Ocean SST anomalies, offering an additional mechanism for the Philippine Sea anticyclone apart from Pacific SST. This anticyclone increases precipitation along the East Asian winter monsoon front from December to May. The anomalous subsidence over the Maritime Continent in conjunction with persistent anomalies of SST and precipitation over the Indian Ocean in spring prevent the northwestward migration of the ITCZ and the associated deep moist layer, causing a significant delay in the Indian summer monsoon onset in June by 6–7 days. At time scales of 5 days, however, the reproducibility of the northward progression of the ITCZ during the onset is low.

Results indicate that Indian Ocean SST anomalies during December through May that develop in response to both atmospheric and oceanic processes to El Niño need to be considered for a complete understanding of regional climate variability, particularly around the Indian Ocean rim.

1. Introduction

Many observational studies show that the El Niño–Southern Oscillation (ENSO) induces substantial sea surface temperature (SST) variations in other tropical oceans. For example, the Indian Ocean witnesses a basinwide warming in boreal winter that peaks in the following spring after the mature phase of El Niño (e.g., Nigam and Shen 1993). Klein et al. (1999) and Murtugudde and Busalacchi (1999) find that surface heat flux is the major mechanism for ENSO-induced warming in the north Indian Ocean. In particular, Klein et al. (1999) showed that changes in atmospheric circulation accompanying El Niño induce changes in cloud cover and evaporation that, in turn, increase the net heat flux entering the remote oceans—the concept of an "atmospheric bridge" that connects SST anomalies in the central equatorial Pacific to those in remote tropical oceans. That mechanism, however, does not explain the SST fluctuations over the southwest Indian Ocean (SWIO) where the anomalies typically reach a maximum (Klein et al. 1999). Xie et al. (2002) and Huang

* International Pacific Research Center Contribution Number 334 and School of Ocean and Earth Science and Technology Contribution Number 6591.

+ Additional affiliation: Department of Meteorology, University of Hawaii at Manoa, Honolulu, Hawaii.

Corresponding author address: Dr. H. Annamalai, International Pacific Research Center/SOEST, University of Hawaii at Manoa, 1680 East–West Road, Honolulu, HI 96822.
E-mail: hanna@hawaii.edu

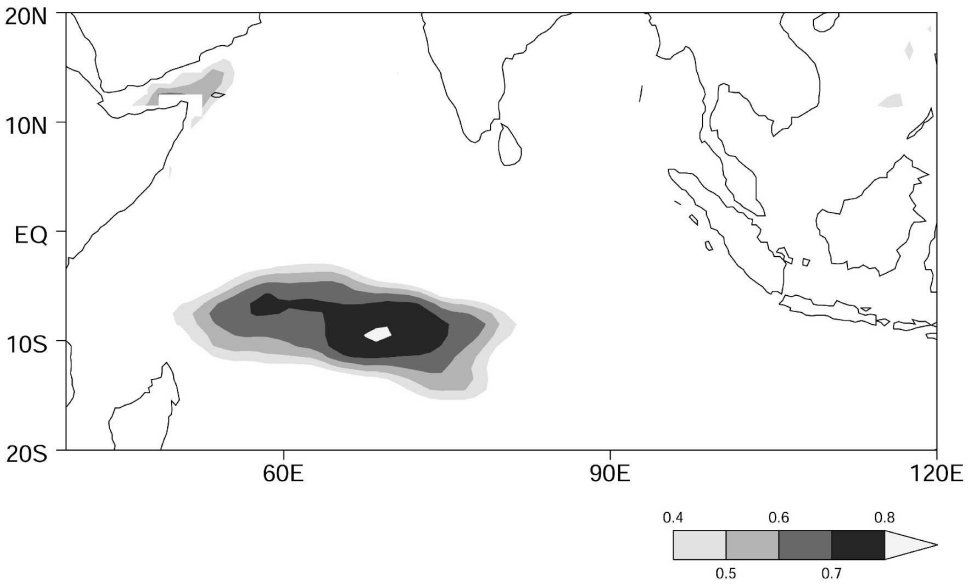

FIG. 1. Simultaneous correlation between anomalous SST and thermocline depth during Dec–May. The depth of the 20°C isotherm represents the thermocline.

and Kinter (2002) demonstrated that much of SWIO SST variability is not locally forced but is due instead to oceanic Rossby waves that propagate from the east. They showed that such a subsurface effect on SST in the SWIO is made possible by the simultaneous presence of mean upwelling and a shallow thermocline dome and further demonstrated that ENSO is the dominant forcing for the SWIO thermocline variability. Xie et al. (2002) noted that, when an El Niño event occurs, anomalous easterlies appear in the equatorial Indian Ocean, forcing a westward-propagating downwelling Rossby wave in the southern Indian Ocean. In summary, both through atmospheric and oceanic processes, El Niño accounts for the basinwide SST variations observed over the tropical Indian Ocean (TIO). Recently, there is renewed interest in all aspects of the coupled system in the tropical Indian Ocean and its role in the regional climate variability (Annamalai and Murtugudde 2004). The present study explores the possible role of the basinwide warming in local and remote effects on the Asian monsoons.

Figure 1 shows the simultaneous correlation between thermocline depth (h) and SST variations during boreal winter and the following spring (December–May), with h represented by the 20°C isotherm depth. The high local correlation confirms the results of Xie et al. (2002) and Huang and Kinter (2002) that subsurface variability exerts a strong influence on SST over SWIO. By analyzing the number of tropical cyclone days during December–April for the period 1951–98, Xie et al. (2002) noted that there are four cyclone days in a year when h is abnormally deep as opposed to only one in a shallow year. Apart from this effect on local climate and due to its persistence for about 6 months, SWIO SST anomalies may influence climate over remote regions—a subject of the present investigation.

During boreal winter of El Niño years, negative convective anomalies over the tropical west Pacific (TWP)–Maritime Continent force an anticyclone in the lower atmosphere over the South China Sea–Philippine Sea region that in turn influences the East Asian winter monsoon (EAWM) (Wang et al. 2000). Observations show that precipitation anomalies along the EAWM front and the anomalous anticyclone over the Philippine Sea persist from boreal winter into the following spring (Harrison and Larkin 1996; Wang et al. 2000). Using an atmospheric general circulation model (AGCM), Wang et al. (2000) showed that the Philippine Sea anticyclone is forced by El Niño and maintained by local air–sea interactions. Lau and Nath (2000) conducted similar sensitivity experiments with a different AGCM and concluded that the existence of the Philippine Sea anticyclone is largely due to tropical Pacific SST anomalies. The AGCM studies of Wang et al. (2000) and Lau and Nath (2000), however, did not consider the effect of Indian Ocean SST anomalies.

ENSO-induced SST anomalies over the Indian Ocean provide a mechanism for the delayed atmospheric response to ENSO after its mature phase. Using a simple linear model forced by Indian Ocean SST

anomalies during boreal winter of El Niño years, Watanabe and Jin (2003) noted that an increase in precipitation over the western Indian Ocean is accompanied with a decrease in precipitation over the TWP – Maritime Continent. Su et al. (2001), again from a simple model, noted a similar precipitation response during the 1997–98 El Niño event. Watanabe and Jin (2003) argued that the suppressed precipitation over the TWP–Maritime Continent strengthens the Philippine Sea anticyclone, in addition to the remote forcing by El Niño–related SST anomalies. These simple linear model results, while appealing, need to be corroborated with more comprehensive AGCM experiments because precipitation interacts with SST and atmospheric circulation in a complex, nonlocal way. Furthermore, Watanabe and Jin (2003) focused only on the boreal winter season and their simple model is not suitable for studying extratropical response, such as EAWM. Finally, sensitivity of the solutions to changes in atmospheric initial conditions cannot be assessed from simple linear models. In the present research, by performing ensemble AGCM simulations we examine if the persistence of SST anomalies over the Indian Ocean influences convective anomalies over the TWP–Maritime Continent and therefore on the EAWM through their effect on the intensity of the Philippine Sea anticyclone.

Another important, yet unresolved issue is the role of Indian Ocean SST in the onset of the Indian summer monsoon (ISM). In their correlation analysis between the ISM onset date and SST anomalies in the preceding winter and spring, Joseph et al. (1994) identified significant positive correlations with SST over SWIO and negative correlations over TWP (Fig. 11 of their paper). From that observational study, Joseph et al. (1994) hypothesized that the SST anomalies over the Indian and TWP oceans cause the interannual variability of the ISM onset through affecting the timing of the northwestward movement of the equatorial convective maximum. Soman and Slingo (1997) used an AGCM and studied the sensitivity of the ISM onset to tropical SST anomalies, focusing on two contrasting years: 1983 (delayed onset) and 1984 (early onset). They concluded that the northward migration of the convective center in spring over the west Pacific is related to in situ SST anomalies and attributed the slow (fast) northward migration in the presence of cold (warm) SST anomalies to the ISM's delayed (early) onset, confirming the Joseph et al. (1994) hypothesis. Their model results, however, did not change significantly after inclusion of Indian Ocean SST anomalies.

Figures 2a–c show the composite pattern of observed SST anomaly difference between years of delayed and early ISM onset during the period 1950–2001. Consistent with Joseph et al. (1994, their Fig. 10), there are warm SST anomalies over the SWIO and equatorial Indian Ocean and cold anomalies over the northern

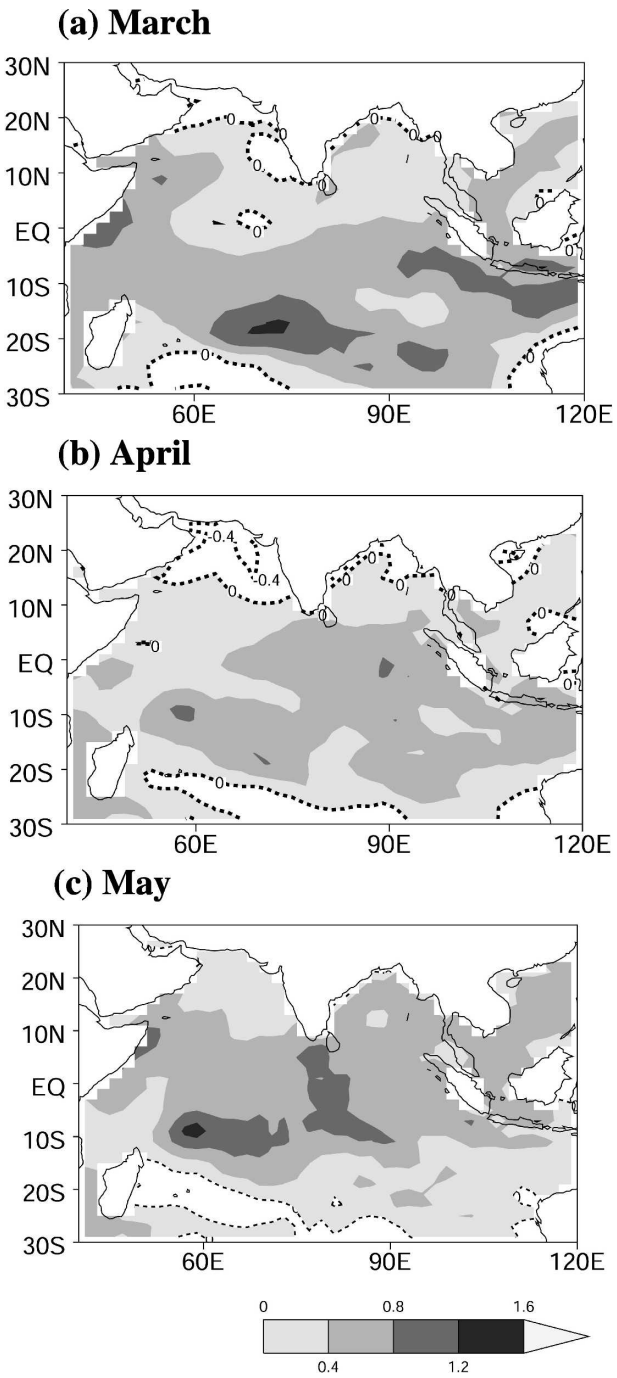

FIG. 2. SST difference (°C) between years of delayed and early ISM onset dates: (a) Mar, (b) Apr, and (c) May. Positive values are shaded progressively, while negative values are shown in dashed contours. The interval is 0.4°C.

Arabian Sea, particularly in April. Even in May, when positive SST anomalies occupy the entire tropical Indian Ocean, the strongest warming is located near and south of the equator. In agreement with Joseph et al. (1994), it is expected that this SST persistence from March to May favors in situ convection over the ocean, thereby delaying the ISM onset over land. Our approach differs from the case studies of Soman and Slingo (1997) in two aspects; namely, we (i) exclusively study the impact of Indian Ocean SST anomalies on the ISM onset by considering more anomalous events and (ii) perform ensemble AGCM integrations to assess the reproducibility of the model results. Our modeling approach can be viewed as an extension of the Joseph et al. (1994) observational study.

The present study investigates the effect of Indian Ocean SST anomalies on local precipitation variations and their remote influence on TWP–Maritime Continent convection, EAWM, and ISM onset. Since the SST anomalies over the tropical Indian Ocean often co-occur with those in the tropical Pacific, it is difficult, if not impossible, to quantify their effects separately from observations alone. On the other hand, experiments with a realistic AGCM forced with SST anomalies in each ocean basin offer a means to separate their effects. We carry out such experiments by forcing an AGCM with prescribed SST anomalies and assess the sensitivity of the results to changes in atmospheric initial conditions by conducting ensemble integrations. Over the regions of interest, the reproducibility of the model-simulated precipitation to changes in model initial conditions is examined.

The main results from our experiments are (i) precipitation variations over the SWIO are induced by local SST anomalies and the reproducibility among the ensemble members is very high; (ii) the basinwide warming of the Indian Ocean alters the Indo–Pacific Walker circulation, affecting TWP convection, the intensity of the low-level anticyclone over South China Sea–Philippine Sea, and the EAWM; and (iii) the persistence of precipitation anomalies over the Indian Ocean affects the northward migration of a deep moist layer and delays the ISM onset by about a week, consolidating the original hypothesis proposed in Joseph et al. (1994). In the model integrations, however, on time scales of 5 days, the reproducibility of the northwestward migration of the convective center during the ISM onset stage is rather poor.

The paper is organized as follows. Section 2 presents the data used and provides a brief description of the AGCM. Section 3 presents the model response in various regions and compares it with observations. Section 4 summarizes our conclusions.

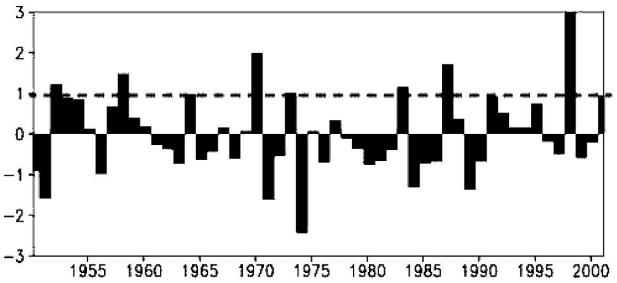

FIG. 3. Time series of SST anomalies (in std dev) averaged over the southwest Indian Ocean (7.5°–17.5°S, 50°–70°E) during Dec of year 0 through May of year 1. The std dev is 0.28°C, and during the period 1950–2001 there are eight strong years (>1.0 std dev). The years 1990–91 and 2000–01 are slightly below the threshold. The eight warm years chosen are (1951–52, 1957–58, 1963–64, 1969–70, 1972–73, 1982–83, 1986–87, and 1997–98). Here year 0 represents the developing phase of El Niño, and all 8 years correspond to moderate to strong El Niño years in the equatorial Pacific.

2. Data and model

a. Data

The atmospheric data used in our study are taken from the National Centers for Environmental Prediction–National Center for Atmospheric Research (NCEP–NCAR) reanalysis for the period 1950–2001 (Kalnay et al. 1996). The atmospheric variables are available at standard pressure levels with a horizontal resolution of 2.5°. We use the Reynolds and Smith (1994) SST product. In addition, we utilize monthly mean rainfall from the Climate Prediction Center (CPC) Merged Analysis Product (CMAP) (Xie and Arkin 1996) for the period 1979–2001. The thermocline depth (h), as represented by the depth of the 20°C isotherm, is taken from the Simple Ocean Data Assimilation (SODA) (Carton et al. 2000). The usefulness of SODA for studying Indian Ocean coupled dynamics has been demonstrated in Xie et al. (2002) and Annamalai et al. (2003).

In our study, monthly mean climatologies are first calculated and anomalies are defined as departures from them. Unless otherwise specified, decadal variability (periods >8 yr) is separated from interannual variability (16 months to 8 years) by harmonic analysis. As an example, Fig. 3 shows the interannual SST anomalies averaged over the SWIO (7.5°–17.5°S, 50°–70°E). Owing to uncertainities in SST observations prior to the satellite era, we examined the monthly observed SST from the Comprehensive Ocean–Atmosphere Data Set (COADS). We constructed the interannual SST anomalies over the SWIO and noted that, apart from the event in 1953, all the other major warm events (Fig. 3) are captured by COADS SST (not shown).

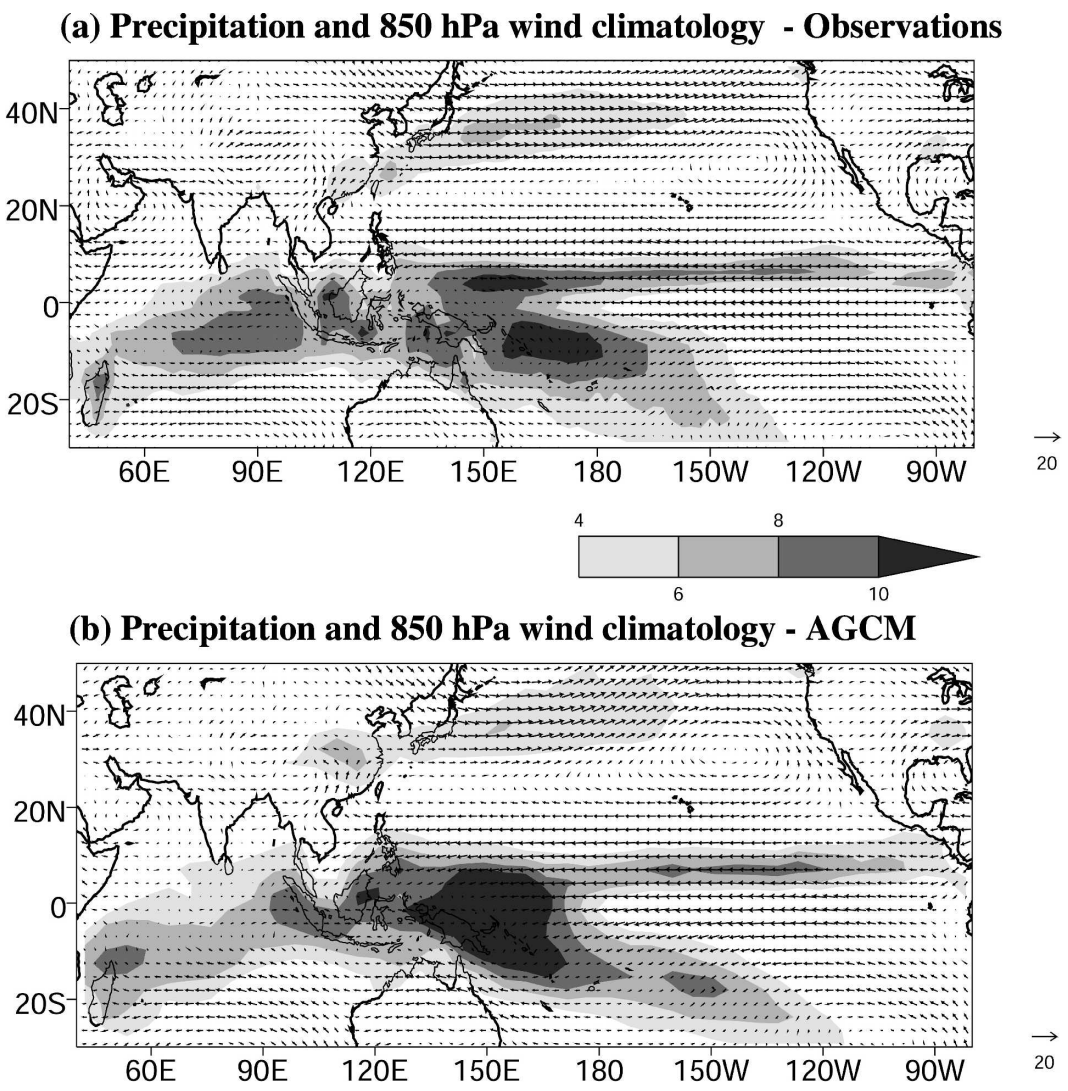

FIG. 4. Seasonal average (Dec–May) precipitation (mm day^{-1}; shown in color shading) and 850-hPa wind climatology: (a) observations and (b) AGCM. The reference wind vector is also shown.

b. Model

We use ECHAM5, the latest Hamburg version of the ECMWF model. It is a global spectral model, which we ran at T42 resolution with 19 sigma levels in the vertical. The nonlinear terms and the parameterized physical processes are calculated on a 128 × 64 Gaussian grid, a horizontal resolution of about 2.8° × 2.8°. As in the earlier version of the model (ECHAM4) (Roeckner et al.1996), the convection scheme is based on the mass flux concept of Tiedtke (1989); the surface fluxes of momentum, heat, and water vapor are based on the Monin–Obukhov similarity theory; and the radiation scheme is from Morcrette et al. (1998). Major changes in the model include implicit coupling of the atmosphere to land surface (Schulz et al. 2001), advective transport (Lin and Rood 1996), a prognostic–statistical scheme for cloud cover (Tompkins 2002), and a rapid-radiative-transfer model for longwave radiation (Mlawer et al. 1997). Model details may be found in Roeckner et al. (2003).

The ECHAM5-simulated climatology, based on a 7-yr mean, is realistic in many aspects. Figure 4 compares precipitation and 850-hPa wind climatology between the model and observations. The Indian Ocean ITCZ is located over the SWIO thermocline dome and is therefore likely to be sensitive to SST changes there. Model/observation differences include (i) overestimation of precipitation intensity along the SPCZ and off Madagascar in the southern Indian Ocean and (ii) un-

TABLE 1. A list of the AGCM experiments discussed in the text.

Expt	Forcing
CTL	Climatological but seasonally varying SST. Duration of the run is 7 yr.
TIP	SST anomalies over the tropical Indo–Pacific regions (30°S–30°N, 40°E–80°W).
TPO	SST anomalies only over the tropical Pacific (30°S–30°N, 120°E–80°W).
TIO	SST anomalies only over the tropical Indian Ocean (30°S–30°N, 40°–120°E).

derestimation of precipitation intensity over the equatorial central Indian Ocean. Despite these differences, the spatial structure and magnitude of precipitation and low-level circulation over the tropical Indo–Pacific (TIP) Oceans are simulated reasonably well. Unless otherwise mentioned, model experiments reported here focus on the two seasons of December–May.

c. Experimental design

We carry out a set of three ensemble experiments. In the tropical Indo-Pacific runs, seasonally varying SST anomalies are imposed in the tropical Indo-Pacific region from 30°S–30°N and seasonally varying climatological SSTs are imposed elsewhere. We refer to them as TIP runs. The tropical Pacific Ocean (TPO) runs are similar to the TIP runs, except that SST anomalies are inserted only in the tropical Pacific. The TIO runs are like the TIP runs, but with SST anomalies imposed only in the tropical Indian Ocean. The set of experiments is expected to reveal the individual and combined effects of SST anomalies on the local and remote climate variability. For example, the difference between TIP and TPO solutions will suggest the effect of Indian Ocean SST anomalies when the Pacific is interactive, while the TIO and TPO solutions indicate the exclusive and noninteractive effect. Table 1 provides some details of the experiments.

For each of the above forcing scenarios, the model is run for seven months from December through June. Monthly surface boundary forcing fields for December–June are obtained by averaging SST anomalies for eight years when December–May mean SST anomalies over the SWIO (Fig. 3) exceed one standard deviation (0.28°C). We choose SWIO SST as our index for two reasons; namely, (i) SST variance reaches a local maximum there and (ii) SST variations are caused by ocean Rossby waves that may be predictable one season in advance (Xie et al. 2002; Huang and Kinter 2002). Over the tropical Indo–Pacific, the composite spatial pattern and intensity of SST anomalies based on the SWIO SST index is nearly identical to that based on El Niño when the December–February mean multivariate ENSO index of Wolter and Timlin (1998) exceeds one standard deviation (not shown).

To account for the atmospheric sensitivity to initial conditions, a 10-member ensemble approach, with changes only in the initial conditions varying from 1 to 10 December but preserving the same SST forcing, are conducted. Initial conditions are taken from the control (CTL) run with the monthly climatological SST as the boundary forcing. In the CTL experiment, the model is run for 7 years. The composites (both constructed from observations and ensembles of AGCM solutions) are subjected to a t test for statistical significance. Values significant at the 95% level or greater are plotted. The level of significance, however, does not alter the main conclusions of the study as long as the interpretations offered are robust and consistent with the dynamics.

In multiple realizations of an AGCM experiment, the reproducibility that is essentially a signal-to-noise ratio is a good measure to asses the model's robustness to the imposed boundary forcing (e.g., Sperber and Palmer 1996). Here, the signal is the variance of the ensemble mean and the noise is the sum of the deviation of the individual member variance from the ensemble mean variance. Reproducibility is related to the F distribution for testing variances of two normally distributed populations. In the present study, we test the signal-to-noise ratio for the model-simulated precipitation, and the more this ratio deviates from 1, the stronger the evidence for unequal population variances. In other words, if the noise is zero, then each realization is an exact replica and the reproducibility is infinity (Sperber and Palmer 1996).

3. Results

a. Observed anomalies

The observed composite SST anomaly pattern (Fig. 5a), not surprisingly, is reminiscent of El Niño. Over the equatorial central–eastern Pacific warm anomalies are flanked by cold anomalies over the TWP, extending into the subtropics in both hemispheres. SST anomalies over the western North Pacific (20°–40°N, 120°–160°E) and including the South China Sea are warmer than normal because of weakened EAWM (Liu et al. 2004). The tropical Indian Ocean displays a basinwide warming with a maximum in the southwest basin. Warm SST anomalies are also present off south Java and over the Indonesian Seas.

Figure 5b shows the associated precipitation anomalies constructed from the last three SWIO warm events (1982–83, 1986–87, and 1997–98) for which CMAP observations over the open oceans are available. For com-

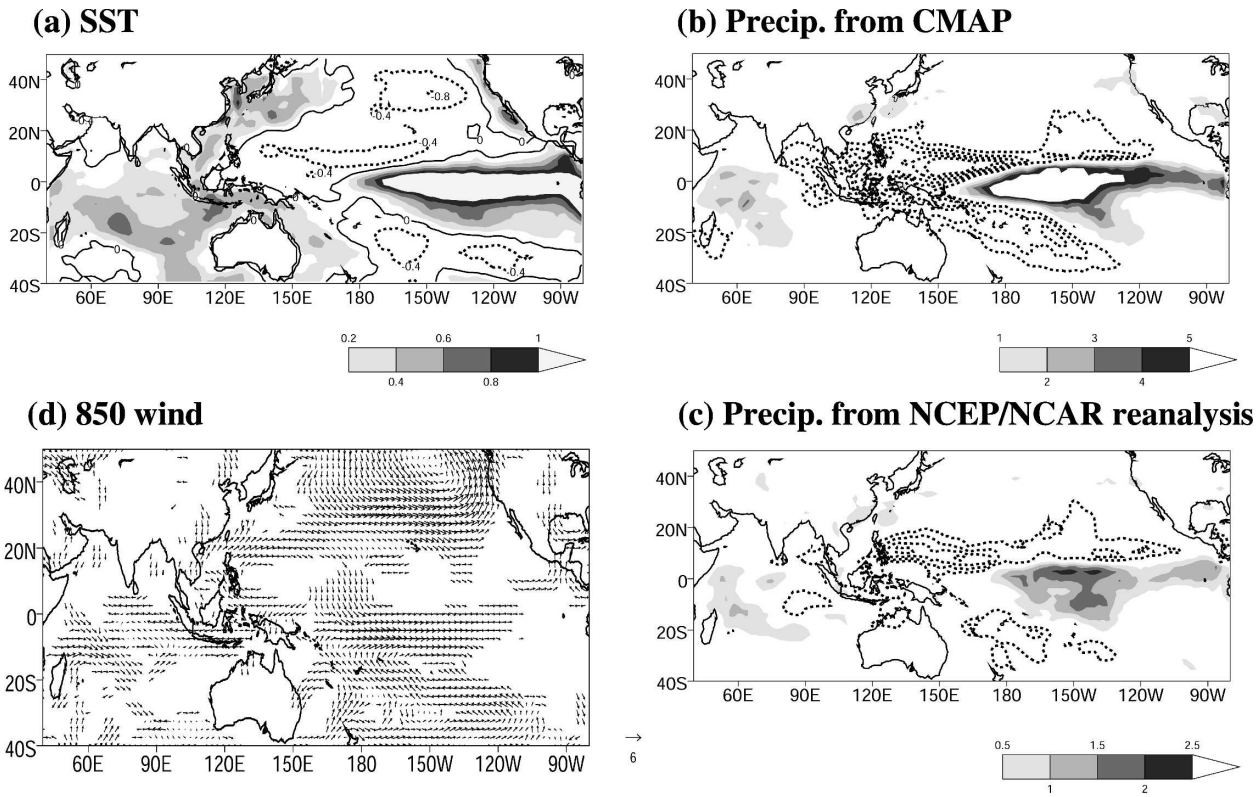

FIG. 5. Seasonal average (Dec–May) composite anomalies: (a) SST (°C), precipitation (mm day^{-1}) from (b) CMAP, (c) NCEP–NCAR reanalysis, and (d) 850-hPa wind (m s^{-1}). The scaling in (c) is different from that in (b). In (a)–(c) positive values are shaded progressively and negative values are shown in contours. The contour interval is (a) 0.4°C, (b) 1 mm day^{-1}, and (c) 0.5 mm day^{-1}.

parison, Fig. 5c shows the corresponding NCEP–NCAR reanalysis precipitation averaged over all the eight events. In general, positive precipitation anomalies are collocated with warm SST anomalies, whereas negative precipitation anomalies overlay warm SST anomalies over the South China Sea, eastern equatorial Indian Ocean, and Indonesian islands extending into north Australia. Model results discussed later (Fig. 6c) suggest that the observed below normal precipitation over these regions is due to subsidence forced by remote convection. As in Su et al. (2001), the reanalysis precipitation during El Niño years (Fig. 5c) is broadly similar to CMAP but the magnitude is weaker. This is possibly due to the difference in the number of samples used in the composites (eight in Fig. 5c to three in Fig. 5b) and to the limitations in the physical parameterizations used in the reanalysis model. Over the Tropics, the 850-hPa wind anomalies (Fig. 5d) are dynamically consistent with the anomalous precipitation patterns. In particular, westerly anomalies over the equatorial central Pacific and easterly anomalies over the equatorial Indian Ocean indicate changes in the Indo–Pacific Walker circulation. Finally, an anomalous anticyclone is prominent in the South China Sea–Philippine Sea region while cyclonic circulation anomalies dominate over the SWIO, both being a Rossby wave response to respective precipitation anomalies nearby (e.g., Gill 1980).

The following three subsections discuss the model response over the SWIO, TWP–Maritime Continent–East Asia, and Indian subcontinent and compare it with observations. Our focus is to understand the role of Indian Ocean SST in these regional climate variations. Therefore, we compare and contrast the model solutions to the SST forcing from individual and combined oceans.

b. Southwest Indian Ocean

Figures 6 and 7 show the model response to tropical Indo–Pacific and Pacific SST anomalies, respectively. Qualitatively, the TIP solutions mimic the observed rainfall and circulation patterns (Fig. 5) over the tropical Indo–Pacific region. In both TIP and TPO solutions, the simulated precipitation and wind anomalies along the equatorial (10°S–10°N) Pacific are broadly similar and agree with observations (Fig. 5). Furthermore, the changes to the equatorial east–west Pacific Walker circulation, as depicted by the upper-level velocity poten-

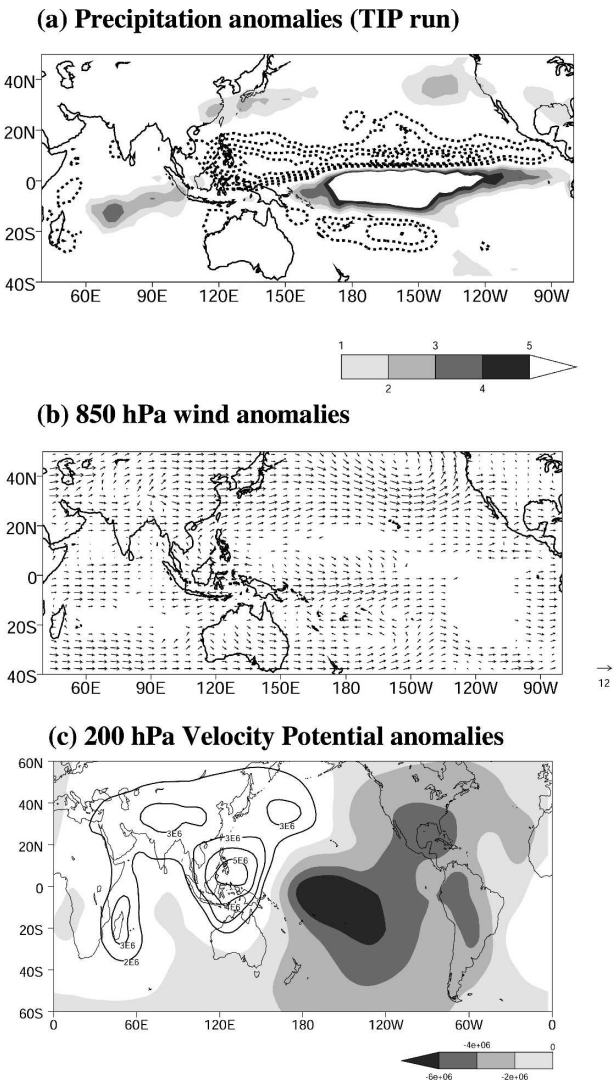

FIG. 6. Seasonal average (Dec–May) (a) anomalous precipitation, (b) 850-hPa wind anomalies, and (c) velocity potential from the TIP solutions. Positive values in (a) are shaded progressively, while negative values are shown in contours with an interval of 1.0 mm day^{-1}. In (c) negative values (ascending regions) are shaded progressively, while positive values (descending regions) are shown as contours with an interval of 1.0×10^6 m^2 s^{-1}.

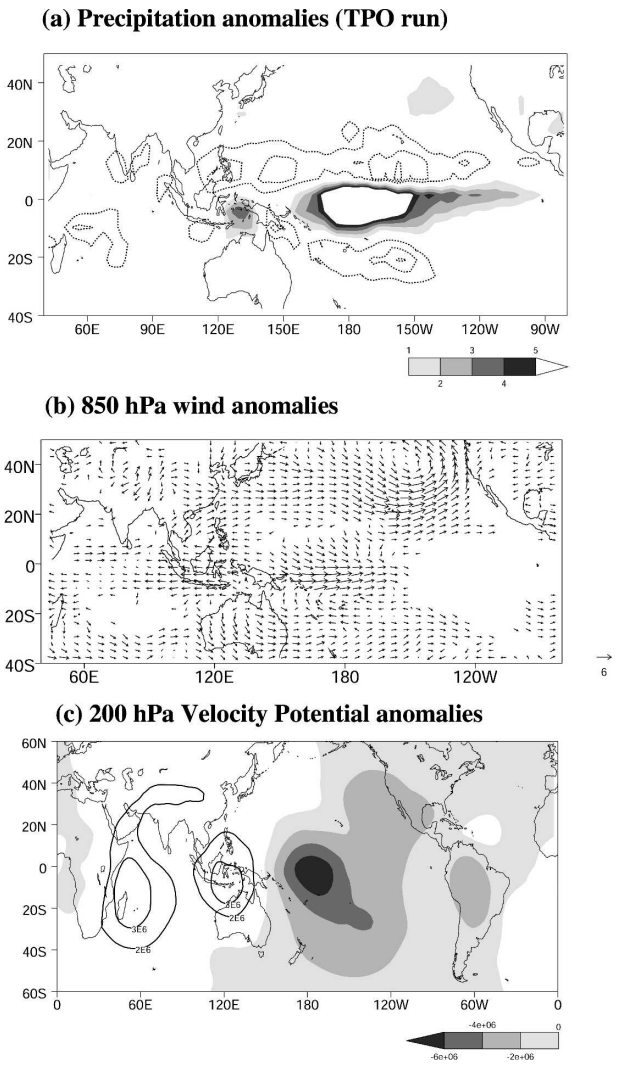

FIG. 7. As in Fig. 6, but for the TPO solutions.

tial, are nearly identical. More importantly, in both the solutions, the reproducibility of the simulated precipitation along the equatorial Pacific is rather striking (Figs. 9c,d). These findings suggest that Pacific SST anomalies are the dominant forcing in determining the atmospheric response there. However, in terms of the strength of the anomalies, prominent differences between the two solutions exist over the TWP–Maritime Continent and along the EAWM region. We return to these issues in section 3c.

Over the tropical Indian Ocean, the large differences between the two solutions highlight the importance of local SST anomalies. In particular, increased precipitation over SWIO in the TIP solutions (Fig. 6a) and the associated ascent (Fig. 6c) are not present in the TPO runs (Fig. 7). In the TIP run, consistent with the precipitation pattern, anomalous westerlies with cyclonic vorticity prevail in the equatorial (15°S–5°N) western Indian Ocean (Fig. 6b), which is much weaker in the TPO run (Fig. 7b). The divergence and associated negative precipitation anomalies off south Java appear in both the TIP and TPO solutions, in agreement with observations. Overall, the wind and precipitation in TIP solutions are in closer agreement with observations than in TPO runs.

The potential role of Indian Ocean SST anomalies on the local and remote effects is further demonstrated by the TIO solution. The spatial distribution of the simu-

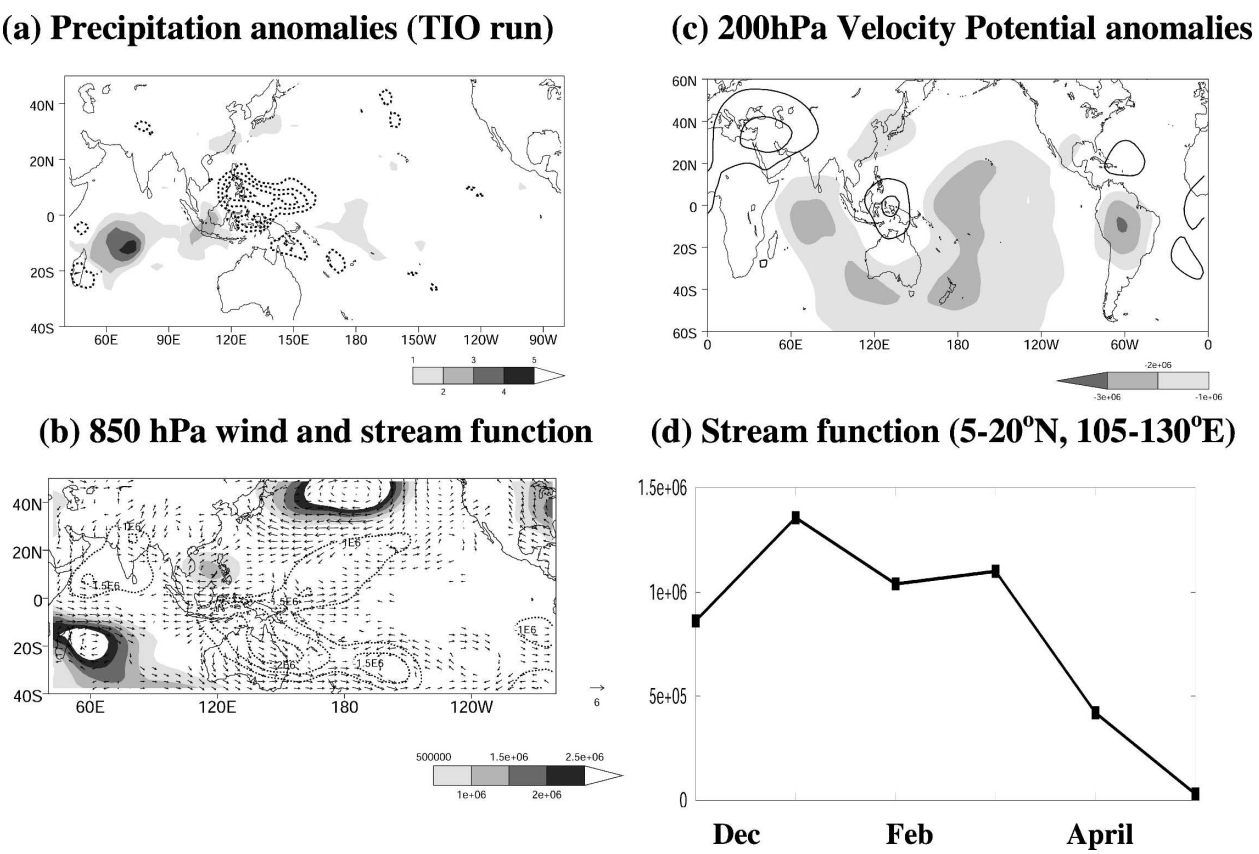

FIG. 8. Seasonal average (Dec–May) (a) anomalous precipitation, (b) 850-hPa wind and streamfunction (positive values shaded and negative values shown in contours) anomalies, (c) velocity potential, and (d) temporal evolution of the anomalous streamfunction averaged over the South China Sea, from the TIO solutions. Positive values in (a) are shaded progressively, while negative values are shown in contours with an interval of 1.0 mm day^{-1}. In (c), negative values (ascending regions) are shaded progressively, while positive values (descending regions) are shown as contours with an interval of 1.0×10^6 m^2 s^{-1}.

lated precipitation anomalies over the SWIO (Fig. 8) agrees well with the observations (Fig. 5b). The simulated low-level circulation anomalies in the TIO runs (Fig. 8b) depict a well-defined cyclone to the southwest of the anomalous precipitation in the southern Indian Ocean. Consistent with Xie et al. (2002) speculation based on observations, these circulation anomalies are a Rossby wave response to the anomalous precipitation (Matsuno 1966; Gill 1980). Compared to TIP runs (Fig. 6a), SWIO precipitation anomalies in the TIO solution are stronger (Fig. 8a), and the sign of the precipitation anomalies are reversed over the equatorial Indian Ocean. These can be attributed to the lack of subsidence induced by tropical Pacific SST warming (Fig. 7c). Therefore, we conclude that local SST anomalies are the dominant factor in determining the precipitation variations over SWIO but not over the equatorial eastern Indian Ocean.

To assess the sensitivity to atmospheric initial conditions, first we show area-averaged precipitation anomalies over the SWIO for all ten members of the ensemble from the TIO runs in Fig. 9a. Despite changes in initial conditions the simulated precipitation anomalies, barring differences in intensity, display the same sign in all the member runs. The dispersion in the simulated intensity among the ensemble members, however, will limit the predictability. To understand this, we show the reproducibility of model-simulated precipitation from all three experiments (Figs. 9b–d). Not surprisingly, the reproducibility over the tropical Pacific in the TIP and TPO simulations is very high. In the TIO solutions, the reproducibility is remarkable over the SWIO, TWP, and EAWM regions. Some recent modeling studies (e.g., Wu and Kirtman 2004) suggest that experiments with prescribed SST anomalies over the Indian Ocean may cause inconsistency between latent heat flux and SST that in turn leads to spurious variance in rainfall and surface wind anomalies, particularly over the northern Indian Ocean during boreal summer. In the present study, the high skill in reproducing the rainfall

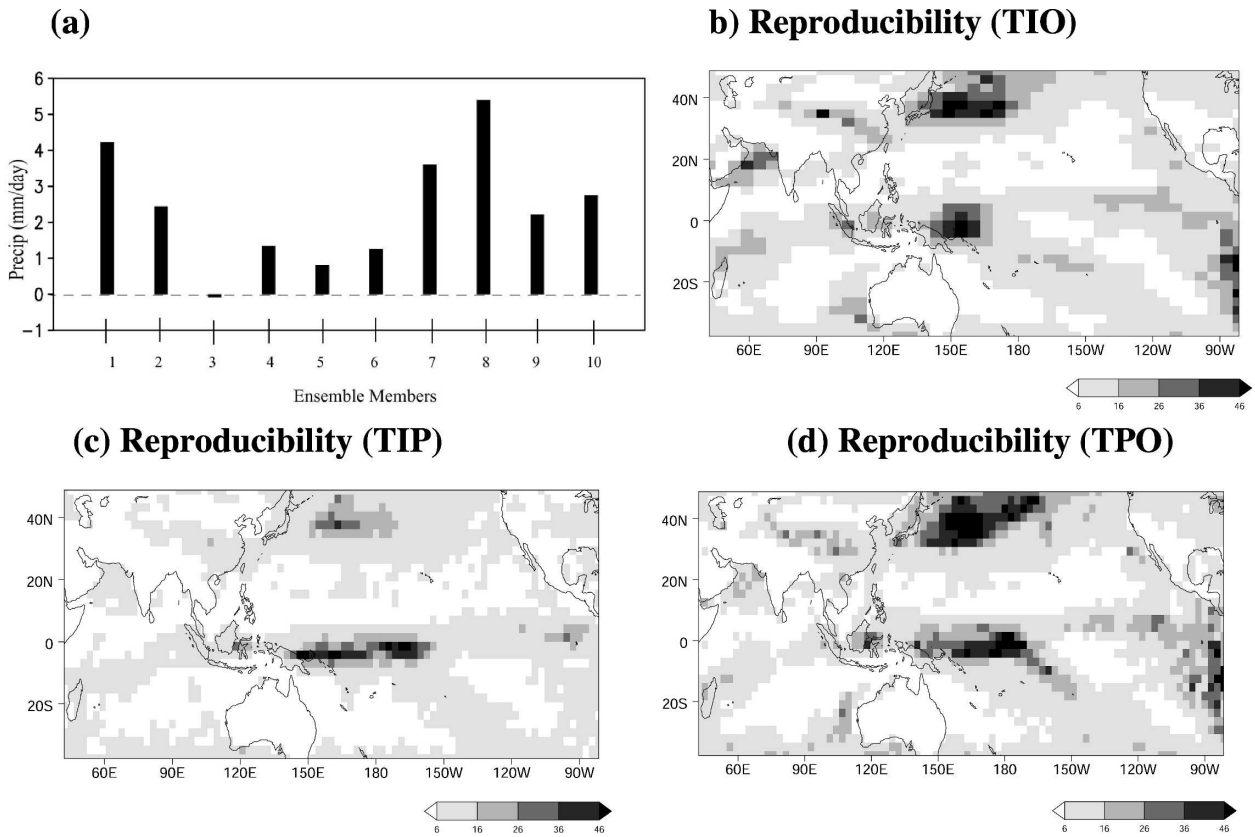

FIG. 9. (a) Precipitation anomalies (mm day^{-1}) averaged over the (b) SWIO (20°S–0°, 55°–85°E) and over the seasons (Dec–May) from the individual ensemble member of the TIO solution. The reproducibility (R) is essentially the signal-to-noise ratio: R is related to the F distribution for testing variances of two normally distributed populations. In (c)–(d) values greater than 6 are significant at 99.9% level.

anomalies over SWIO (Fig. 9) implies that the conjecture of Wu and Kirtman (2004) may depend on the seasons, regions where SST anomalies are largely flux driven, and also the mean state of the models employed. Other studies indicate that the potential predictability of seasonal means (signal) is limited by the chaotic intraseasonal and synoptic variability (noise), again during boreal summer (e.g., Sperber et al. 2000; Krishnamurthy and Shukla 2000). Over the SWIO, despite pronounced observed tropical cyclone activity during December–May (Jury et al. 1999), the reproducibility of seasonal rainfall anomalies by ECHAM5 is encouraging. Sensitivity experiments with ECHAM 4.6, an earlier version to ECHAM5, produced similar results (not shown). This, along with the fact that ocean Rossby waves excited in the eastern basin take a few months to cross the basin (Xie et al. 2002; Huang and Kinter 2002), suggests that SST and rainfall variations in the SWIO may be predictable a few months in advance. We are currently investigating the robustness of the results with other AGCMs and are examining the relationship between latent heat flux and SST, and the results will be reported elsewhere. Here, the reproducibility of the precipitation anomalies over SWIO (Fig. 9b) is appealing, and therefore the possible effect of Indian Ocean SST on remote climate is expected to be realistic.

c. *Tropical West Pacific and East Asian winter monsoon*

This subsection discusses the effect of Indian Ocean SST on the EAWM, primarily through its influence on TWP convection and the associated anomalous Philippine Sea–South China Sea anticyclone. A comparison of the precipitation simulation between the TIP (Fig. 6) and TPO solutions (Fig. 7) demonstrates the potential effect of Indian Ocean SST anomalies on the TWP convection. This can be further delineated from the TIO solutions (Fig. 8a) where increased precipitation over the western Indian Ocean is accompanied with a substantial decrease (4–5 mm day^{-1}) over the TWP–Maritime Continent.

The interpretation for the above notable precipitation difference is that in the TIP solutions convection

induced by equatorial Pacific and Indian Ocean warming enhances subsidence over the TWP–Maritime Continent region (Fig. 6c). This subsidence, in conjunction with local cold SST anomalies (Fig. 5a), results in stronger negative precipitation anomalies (~6–7 mm day^{-1}; Fig. 6a). Similarly, in the TIO runs, warm SST anomalies increase the convection over SWIO, and the resultant heat source forces low-level (upper-level) easterly (westerly) wind anomalies over the equatorial eastern Indian Ocean and west Pacific as a Kelvin wave response (Fig. 8b). Consistent with Watanabe and Jin (2003), our model results suggest that the changes in the Indian Ocean Walker circulation (Fig. 8c) induce subsidence and reduce the precipitation over the TWP–Maritime Continent. As a consequence, the anomalous anticyclone over the South China Sea persists from December through May (Fig. 8d). In the TPO runs, subsidence induced by Indian Ocean warming is absent (Fig. 7c). Therefore, the magnitude of the negative precipitation anomalies over TWP–Maritime Continent is rather weak (2–3 mm day^{-1}; Fig. 7a). One can infer either from the difference (TIP minus TPO) or from the TIO solutions that more than 50% of the precipitation anomalies over the TWP–Maritime Continent region is due to Indian Ocean SST anomalies. As a consequence, both in the TIP and TIO solutions the low-level climatological mean flow (Fig. 4) over the South China Sea is enhanced by the anomalous southerlies (Figs. 6b and 8b). The net result is the intensification of the rainfall along the EAWM front in both solutions (Figs. 6a and 8a). We conclude that, even without tropical Pacific SST forcing, the South China Sea–Philippine Sea anticyclone still develops (Fig. 8b) and persists (Fig. 8d) and the rainfall along the EAWM front to the north is also strengthened in response to Indian Ocean warming.

While Wang et al. (2000) and Lau and Nath (2000) stressed the importance of equatorial central–eastern Pacific and local SST anomalies for the Philippine Sea anticyclone, our model results indicate that the subsidence induced by the delayed warming in the Indian Ocean in response to ENSO is an additional mechanism for the suppression of precipitation over the TWP–Maritime Continent and the Philippine Sea anticyclone. In our earlier study (Annamalai et al. 2005), it is noted that the formation of the Philippine Sea anticyclone during boreal fall of El Niño years is also sensitive to the spatial distribution of SST anomalies in the tropical Indian Ocean.

Apart from the model basic state, the model's precipitation response to prescribed SST anomalies depends on the mean SST over the respective regions. For example, during December–May the mean SST over the SWIO lies between 29° and 30°C (not shown) and warm anomalies of 0.5°C will have a significant impact on precipitation due to the nonlinear relationship between SST and convection (Graham and Barnett 1987). In contrast, the mean SST over the winter South China Sea and along the EAWM front is around 25°–26°C (not shown), and with moderate warm anomalies there the total SST does not exceed 28°C, the threshold necessary to support the occurrence of deep convection. Therefore, the remote forcing from the Indian Ocean becomes important.

From observations, Wang et al. (2000) showed that precipitation anomalies along the EAWM front and the anomalous anticyclone over the Philippine Sea persist from boreal winter into the following spring. It should be noted that the tropical mean state is considerably different between boreal winter [December–February (DJF)] and spring [March–May (MAM)]. DJF surface flow in the South China Sea is dominated by the northeast monsoon. Observed surface winds start to turn southwesterly in late May (see Fig. 2 in Kawamura et al. 2001). Therefore, a division into DJF and MAM is necessary in light of the background wind. Figures 10a–b show the simulated precipitation anomalies from the TIO runs separately for the two seasons. The corresponding observed precipitation anomalies from CMAP are shown in Figs. 10c and 10d, respectively. Despite the changes in the background state the spatial distribution of negative precipitation anomalies over the TWP and EAWM regions persists. The intensity of precipitation anomalies, however, is slightly stronger during boreal winter (Figs. 10a,c). Similar results are noticed in the TIP solutions (not shown).

d. Indian summer monsoon onset

This subsection discusses the role of Indian Ocean SST in delaying the northward migration of the deep moist layer associated with the ISM onset. Traditionally, the India Meteorological Department declares the ISM onset based on rainfall over the southern tip of India, and according to this criterion the climatological onset date is 31 May (Joseph et al. 1994). Figure 11a shows the departure in the ISM onset dates for the period 1950–2001. In 5 out of 8 years when anomalous SWIO warming exceeds one standard deviation (Fig. 3), the ISM onset date is delayed. If one uses a 0.75 standard deviation as the SST threshold (Fig. 3), then the onset is delayed in 8 out of 12 years. In some years, such as 1972 and 1997 (Fig. 11a), the onset is delayed during the developing phase of El Niño, while in the majority of the years the onset delay occurs following the mature phase of El Niño, consistent with the findings of Joseph et al. (1994).

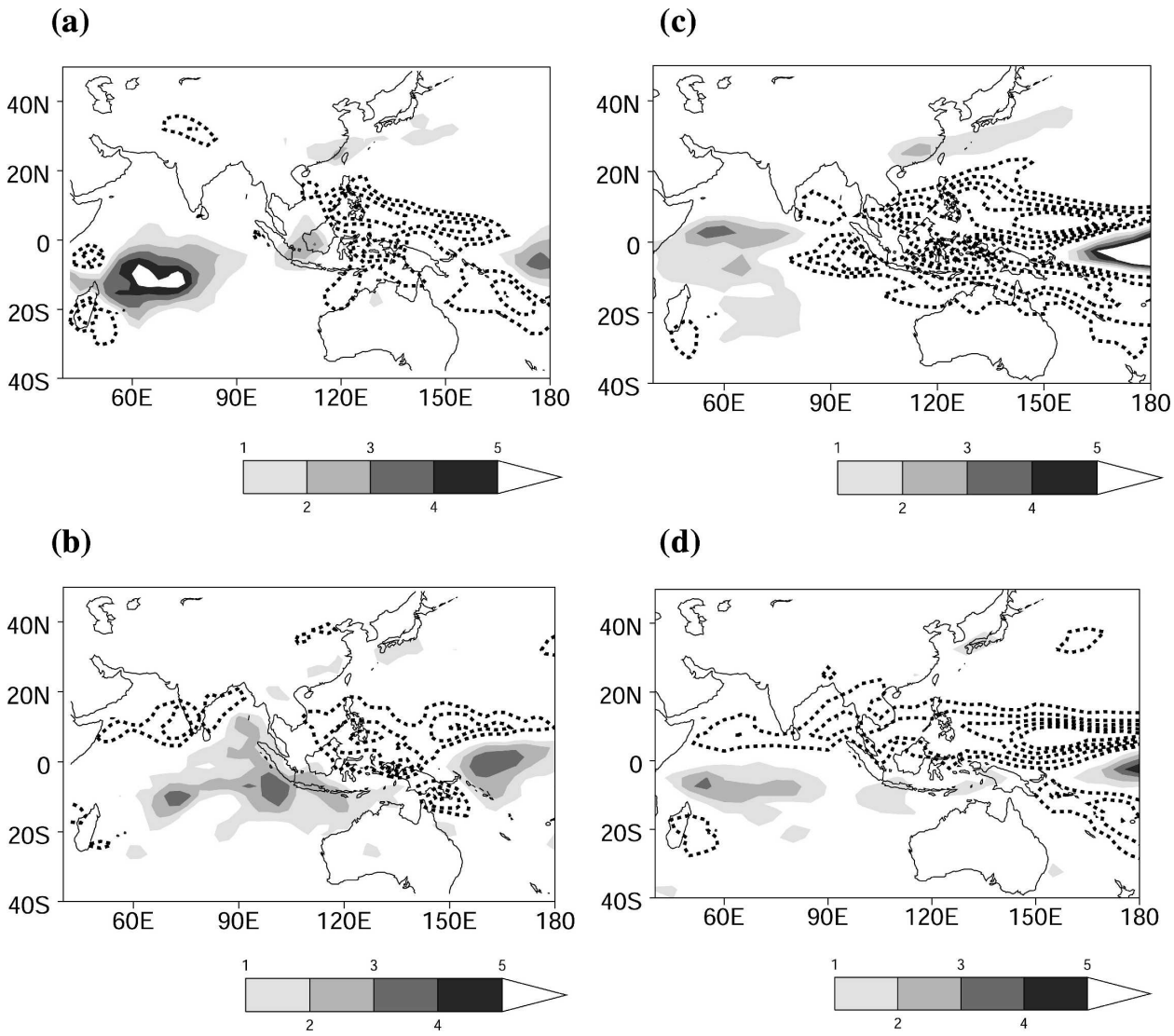

FIG. 10. Seasonal average precipitation anomalies (mm day^{-1}) during DJF (a) TIO runs and (c) observations and during MAM (b) TIO runs and (d) observations. Positive (negative) values are shaded progressively (contours). Contour interval is 1.0 mm day^{-1}.

It is well known that during the onset stage dramatic changes in the large-scale atmospheric pattern occur over the monsoon domain. Approximately 3–5 days prior to the rapid increase in rainfall over southern India there is a dramatic rise in the kinetic energy over the Arabian Sea (e.g., Krishnamurti 1987). This increase in kinetic energy is associated with the development of the low-level jet known as the Findlater Jet (Joseph and Raman 1966; Findlater 1969). During the onset, the axis of the jet lies around 5°–12°N (Joseph and Sijikumar 2004), and therefore the kinetic energy averaged over the region (5°–12°N, 50°–70°E) and exceeding a threshold of 80 m^2 s^{-2} is referred to as the dynamical onset here (Fig. 12). Soman and Krishnakumar (1993) showed that the ISM onset is associated with large-scale increases in atmospheric moisture content. In particular, the moist layer, originally confined to the boundary layer, deepens considerably. Hence, the north-northwestward migration of vertically integrated moisture is a good measure of the poleward migration of the ITCZ from the equatorial region toward the monsoon domain (Figs. 13–14). Finally, we assess the reproducibility of the northwestward progression of the simulated precipitation (Fig. 15). The results are based on a 7-yr mean and individual years for the CTL run, and a 10-member ensemble mean and individual members for the sensitivity runs.

Figure 12 shows the temporal evolution of the kinetic energy from the CTL (Fig. 12a) and the sensitivity (Figs. 12b–d) runs, respectively. In the CTL run, the

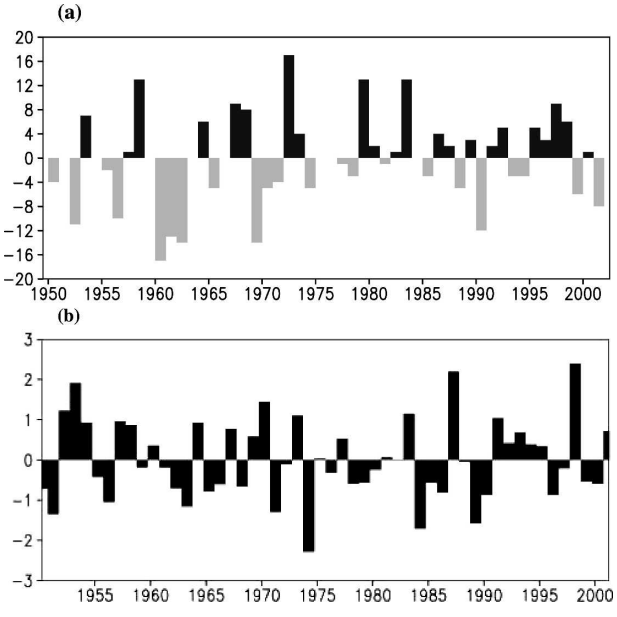

FIG. 11. (a) Time series of ISM onset dates shown as departures from normal onset date of 31 May. The delayed (early) onset dates are shown in dark (light) shading. Out of the eight warm years chosen in the present study (Fig. 2), the onset is delayed in five years (1958, 1964, 1973, 1987, and 1998). (b) Time series of SST anomalies (in std dev) averaged over SWIO (7.5°–17.5°S, 50°–70°E) during MAM. The std dev is 0.29°C.

7-yr mean kinetic energy (thick red line) gradually rises around 22 May with an abrupt increase around 3 June. The mean model dynamical onset is consistent with other AGCMs (e.g., Krishnamurti 1987; Soman and Slingo 1997). Out of the seven years considered here, in four years the raise in kinetic energy is well before the end of May. In the remaining three years, the delay is prominent in one case when the onset occurs around 10 June. In contrast, in years when warm SST anomalies persist over the SWIO, the mean dynamical onset (thick red line) occurs at about 7 June (Fig. 12b), one week later than in the CTL run. This delay in the onset simulated by the model agrees with observations (Fig. 11a). In the TIO runs, the onset is earlier only in two cases, and the solutions from the majority of the ensemble members converge toward a systematic delay. In the TPO solutions, the mean onset (thick red line) occurs a few days earlier than in the CTL run, although the onset is delayed in three members. Among all the solutions, the extreme delay in the onset (around 20 June) occurs in one of the members in the TPO solutions. In the TIP, only five members indicate a delay (Fig. 12d), and the ensemble mean (thick red line) suggests a late onset by 2–3 days only. In summary, the delay in the ISM onset in the ECHAM5 model is sen-

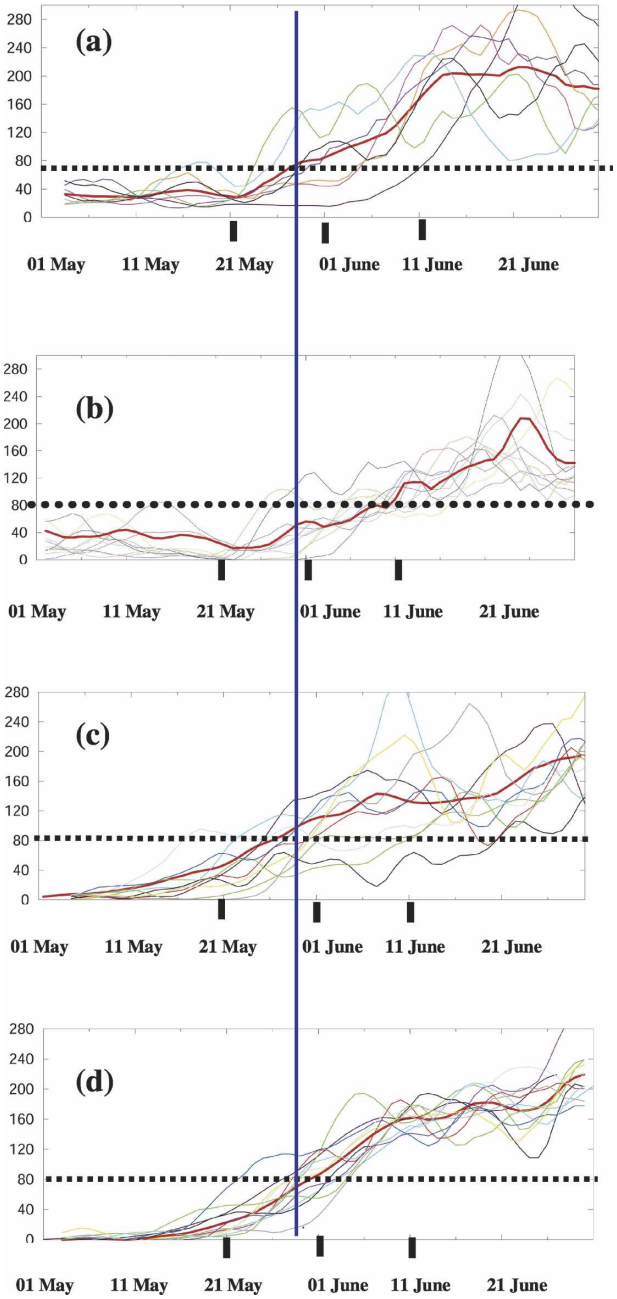

FIG. 12. Time series of kinetic energy (KE: in $m^2 s^{-2}$) averaged over the Arabian Sea (5°–12°N, 50°–70°E) from (a) CTL, (b) TIO, (c) TPO, and (d) TIP solutions, respectively. The dotted line represents the threshold value of 80 ($m^2 s^{-2}$), and the date when the KE exceeds the threshold is considered as the model dynamical onset date. In (a) the KE from the individual years as well as their mean (thick red line) are shown. For all the sensitivity runs, the KE from the individual members as well the ensemble mean (thick red line) are shown. A 5-day running mean is applied in all the cases. The vertical line corresponds to onset in the CTL run.

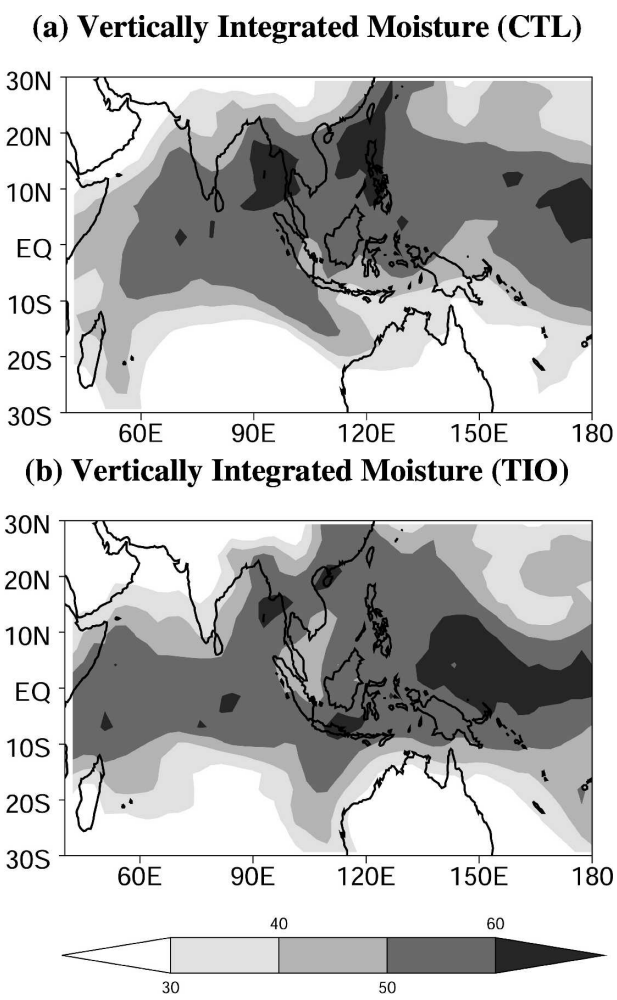

FIG. 13. Vertically integrated (1000 to 100 hPa) specific humidity (kg m^{-2}) averaged over three days centered on 20 May from the (a) CTL run and (b) TIO solutions.

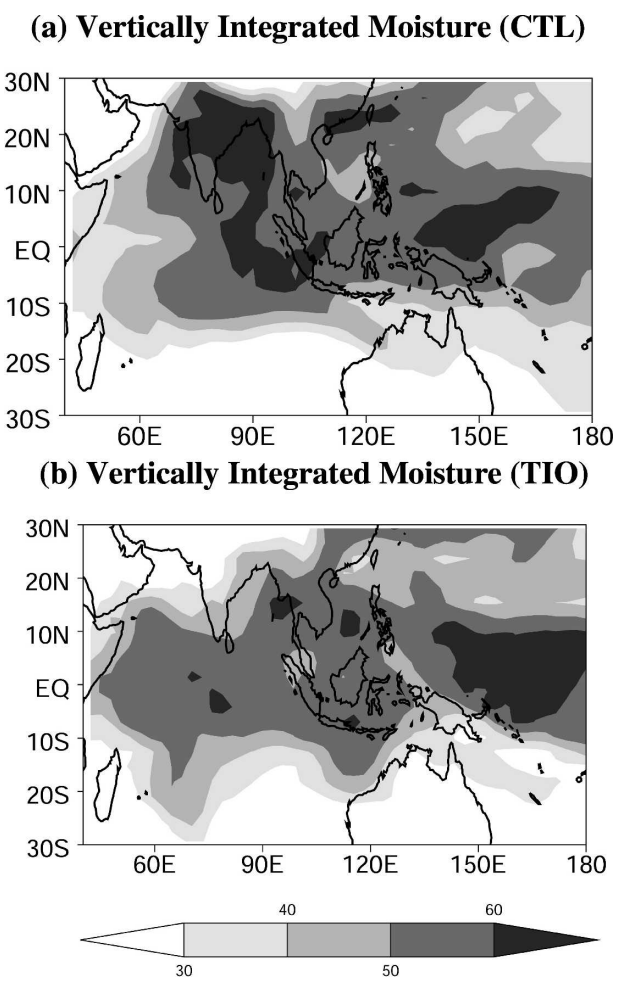

FIG. 14. As in Fig. 13, but centered on 1 Jun.

sitive to Indian Ocean SST anomalies—a result that needs to be verified with other AGCMs.

To understand the large-scale moisture distribution before and during the climatological onset (e.g., Fig. 12a), column-integrated moisture averaged for 3 days centered on 20 May and 1 June are shown in Figs. 13 and 14, respectively. On 20 May, high moisture content (>50 kg m^{-2}) occupies a large region encompassing the equatorial Indian Ocean, Bay of Bengal, South China Sea, and the southern tip of India in the CTL run (Fig. 13a), conditions favorable for ISM onset. In sharp contrast, in the TIO solutions (Fig. 13b), high moisture content is confined to the near-equatorial Indian Ocean, eastern Bay of Bengal, and near-equatorial western Pacific while the southern tip of India is relatively dry. On 1 June (Fig. 14) in the CTL run, the deep moist layer has moved north-northwestward to cover the entire Indian subcontinent, with a maximum over the head of the Bay of Bengal. In particular, the east–west-oriented monsoon trough along 20°–25°N is rich in moisture (>60 units), heralding the establishment of the monsoon. In contrast, high moisture content is yet to reach the southern tip of India in the TIO solutions on 1 June (Fig. 14b), conditions typical of preonset. By comparing the moisture distribution over the tropical western Pacific (Figs. 13b and 14b), it is found that high moisture content stalls over the equatorial west Pacific. The changes in the moisture are consistent with the meridional dipole of precipitation during spring (Fig. 10) with positive and negative anomalies over the equatorial and northern Indian Ocean, respectively. This feature again suggests a delay in the northward movement of the ITCZ. Based on strong minus weak ISM year composites Kawamura et al. (2001) note a similar antisymmetric rainfall pattern about the equator during boreal spring from observations.

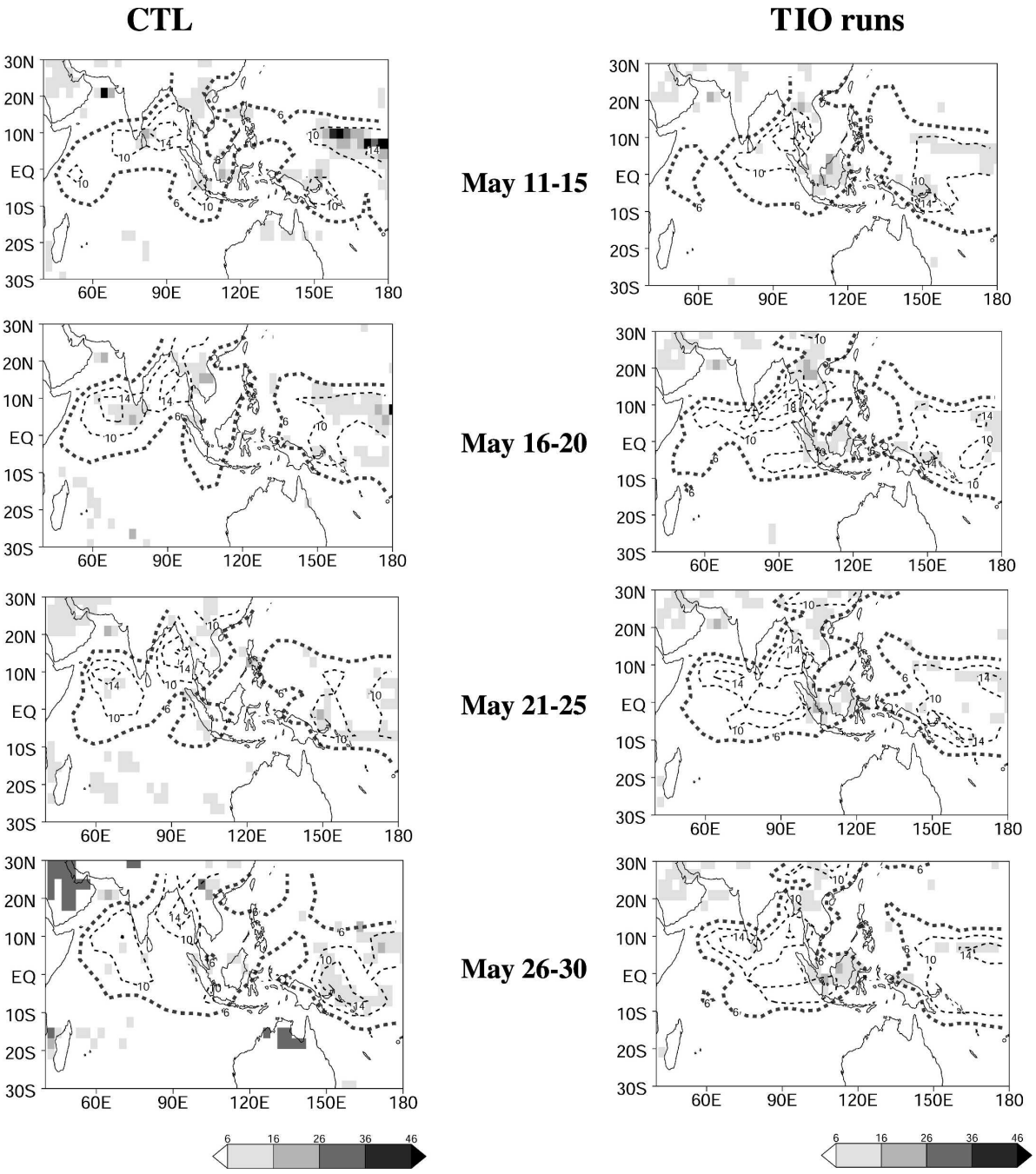

FIG. 15. Pentad mean precipitation (mm day^{-1}; in contours) for pentads prior to and during the ISM onset from the (left) CTL and (right) TIO runs. The 6 mm day^{-1} contour corresponding to 240 W m^{-2} of OLR is shown by the thick broken line. The contours 10, 14, and 18 mm day^{-1} correspond to 220, 200, and 180 W m^{-2} of OLR, respectively. The contour values are chosen to represent "deep convection" associated with the ISM onset. Also shown is the reproducibility (shaded), and values >6 are significant at the 95% (99.9%) level for the CTL (TIO) runs. The reproducibility patterns in the TIO runs do not change for significance at the 95% level.

Among all solutions, the dispersion in the strength of the kinetic energy among the members is higher in the TPO and CTL than in the TIO and TIP runs (Fig. 12). One interpretation is that the inclusion of Indian Ocean SST anomalies possibly reduces the "noise" due to internal variability of the atmosphere. To quantify this, we examine the reproducibility in the spatiotemporal evolution of the large-scale ITCZ prior to the onset in the TIO and CTL runs.

Figure 15 shows the evolution of 5-day mean precipi-

tation (contours) and its reproducibility (shaded) from the CTL and TIO solutions. In the observational study, Joseph et al. (1994) noted that at the time of the ISM onset deep convection ($\sim$10 mm day^{-1} of rainfall) is increased in a band about 5°–10° meridionally, extending from the south Arabian Sea to south China longitudinally (see Fig. 5 of their paper). Such large-scale features of the ITCZ are present in the model simulations. Compared to the CTL solutions, in the TIO solutions there is a systematic delay of about 5 days in the northwestward progression of the ITCZ. In contrast, the reproducibility of the pentad mean precipitation (shaded, Fig. 15) along the ITCZ, in both runs, barely passes the significance levels. This low skill compared to the seasonal mean reproducibility discussed earlier (Fig. 9) implies that the noise contribution by the atmospheric internal variability at shorter time scales is large over the monsoon region. Further modeling studies with more ensemble members are required to address this issue.

In summary, when warm SST anomalies persist near and south of the equator in the Indian Ocean in boreal spring, there is a delay in the northward migration of the deep moist layer and in the formation of the Findlater Jet. In a case study of the 1983 ISM onset, Soman and Slingo (1997) noted a 5–7-day delay in the dynamical onset over the Arabian Sea and argued that cold SST anomalies over the TWP caused the delay in the northward migration of the convective maximum. Our model results, however, indicate that to a considerable degree, convective anomalies over the TWP are influenced by Indian Ocean SST anomalies (Fig. 8a). Therefore, either directly affecting the local precipitation or remotely modulating the TWP convection or both, warm SST anomalies that occur over the Indian Ocean after the mature phase of El Niño can delay the ISM onset. The ISM onset is also sensitive to the phase of the Madden–Julian oscillation (e.g., Flatau et al. 2001) and to the developing phase of El Niño (e.g., 1972; Joseph et al. 1994). Furthermore, recent studies note a weakening in the ENSO–monsoon relationship and attribute that weakening to global warming (Krishnakumar et al. 1999; Ashrit et al. 2001). Therefore, it will be interesting to study the impact of global warming on the ISM onset, both during the developing phase and after the mature phase of El Niño.

4. Summary and discussions

The present study investigates the effect of tropical Indian Ocean SST anomalies, in particular the basinwide warming that occurs after the mature phase of El Niño, on regional climate variability over the SWIO, the TWP–Maritime Continent, the EAWM, and the ISM. We focus on two seasons from December through May. We have conducted three 10-member ensemble simulations with an AGCM in which SST anomalies are prescribed as the lower boundary condition in the Indian basin, the Pacific basin, and their combined domain, respectively.

Qualitatively, the TIP solutions reproduce the observed anomaly patterns of rainfall and low-level circulation over the tropical Indo–Pacific (Fig. 6). The importance of Indian Ocean SST anomalies in determining the local and remote precipitation and circulation anomalies is illustrated by a comparison between the TIP and TPO solutions (Figs. 6 and 7) and the TIO runs (Fig. 8). Our model solutions demonstrate that the precipitation anomalies over the SWIO are largely forced by local SST anomalies and that this local response is robust and highly reproducible (Fig. 9). Our model results reaffirm the conclusions of Shukla (1998) that at seasonal and longer time scales the underlying SST largely determines tropical rainfall patterns, particularly over the open oceans.

Indian Ocean SST exerts a significant influence on climate in remote regions. We estimate that about 50%–60% of precipitation anomalies over the TWP–Maritime Continent region are forced by Indian Ocean SST anomalies. Consistent with this precipitation response, the low-level South China Sea–Philippine Sea anticyclone that forms at the mature phase of El Niño and persists afterwards is well defined in both the TIP and TIO runs (Figs. 6 and 8). The development of this anticyclonic circulation leads to increased rainfall along the EAWM front. Finally, our model results suggest that the SWIO warming effect lingers into early summer and causes a significant delay in the ISM onset by a week (Figs. 12–15). With positive SST anomalies near and south of the equator convection stays over the ocean longer than normal, keeping the ITCZ from advancing into the Indian subcontinent. Our model solutions confirm the hypothesis embodied in Joseph et al. (1994). However, during the ISM onset stages the reproducibility of the pentad mean precipitation is rather poor. Our conclusions are, however, based on ECHAM model solutions, and therefore some caution needs to be exercised on the results that might be model dependent. We are currently investigating the reproducibility of this result with other AGCMs.

Variance of equatorial eastern Pacific SST peaks in December and decays rapidly in the following season. This and other recent studies, however, show that ENSO effects linger much longer. This calls for mechanisms for delayed ENSO effect long after SST anomalies have dissipated over the eastern equatorial Pacific.

Wang et al. (2000) emphasized the importance of local air–sea interactions in maintaining the Philippine Sea anticyclone following El Niño. In response to ENSO, Indian Ocean SST warming peaks in boreal spring, a delay due to the thermal inertia of the ocean mixed layer (e.g., Lau and Nath 2000) and propagation of ocean Rossby waves (Xie et al. 2002). Our AGCM results demonstrate that the subsidence induced by delayed SST response in the Indian Ocean to ENSO forcing is an additional mechanism for the Philippine Sea anticyclone. Our results extend those of Soman and Slingo (1997) and suggest that the convective anomalies over the tropical west Pacific are also modulated by Indian Ocean SST anomalies in spring, thereby stressing the role of Indian Ocean SST anomalies in the ISM onset delay. This recognition of the Indian Ocean as a condenser in climate response to ENSO calls for further studies of its dynamics and interaction with the atmosphere and teleconnection out of the ocean basin. On this line of interest, we will be examining the possible role of Indian Ocean SST anomalies in influencing the Northern Hemispheric circulation in a future study.

Acknowledgments. H. Annamalai appreciates the discussions with Prof. J. Shukla and Dr. H. Nakamura. Some comments from Drs. R. Krishnan and Justin Small on the draft version of the manuscript are appreciated. This research is partly funded by the Japan Agency for Marine-Earth Science and Technology (JAMSTEC) through its sponsorship of the International Pacific Research Center (IPRC), NOAA CLIVAR Pacific Program, and NSFC (Grant 40240420564). Comments from Dr. Martin Hoerling, the editor, and the anonymous reviewers helped improve the manuscript.

REFERENCES

Annamalai, H., and R. Murtugudde, 2004: Role of the Indian Ocean in regional climate variability. *Earth's Climate: The Ocean-Atmosphere Interaction, Geophys. Monogr.,* No. 147, Amer. Geophys. Union, 213–246.

——, ——, J. Potemra, S. P. Xie, P. Liu, and B. Wang, 2003: Coupled dynamics in the Indian Ocean: Spring initiation of the zonal mode. *Deep-Sea Res.,* **50B,** 2305–2330.

——, S. P. Xie, J. P. McCreary, and R. Murtugudde, 2005: Impact of Indian Ocean sea surface temperature on developing El Niño. *J. Climate,* **18,** 302–319.

Ashrit, R. G., K. Rupakumar, and K. Krishnakumar, 2001: ENSO-monsoon relationship in a greenhouse warming scenario. *Geophys. Res. Lett.,* **28,** 1727–1730.

Carton, J., G. Chepurin, X. Cao, and B. Giese, 2000: A simple ocean data assimilation analysis of the global upper ocean 1950–95. Part I: Methodology. *J. Phys. Oceanogr.,* **30,** 294–309.

Findlater, J., 1969: A major low level current near the Indian Ocean during northern summer. *Quart. J. Roy. Meteor. Soc.,* **95,** 400–403.

Flatau, M. K., P. J. Flatau, and D. Rudnick, 2001: The dynamics of double monsoon onsets. *J. Climate,* **14,** 4130–4146.

Gill, A. E., 1980: Some simple solutions for heat-induced tropical circulation. *Quart. J. Roy. Meteor. Soc.,* **106,** 447–462.

Graham, N. E., and T. P. Barnett, 1987: Sea surface temperature, surface wind divergence, and convection over tropical oceans. *Science,* **258,** 657–659.

Harrison, D. E., and N. K. Larkin, 1996: The COADS sea level pressure signal: A near-global El Niño composite and time series view, 1946–1993. *J. Climate,* **9,** 657–659.

Huang, B. H., and J. L. Kinter III, 2002: Interannual variability in the tropical Indian Ocean. *J. Geophys. Res.,* **107,** 3199 doi:10.1029/2001JC001278.

Joseph, P. V., and P. L. Raman, 1966: Existence of low-level westerly jet stream over peninsular India during July. *Indian J. Meteor. Geophys.,* **17,** 407–410.

——, and S. Sijikumar, 2004: Intraseasonal variability of the low-level jet stream of the Asian summer monsoon. *J. Climate,* **17,** 1449–1458.

——, J. K. Eischeid, and R. J. Pyle, 1994: Interannual variability of the onset of the Indian summer monsoon and its association with atmospheric features, El Niño, and sea surface temperature anomalies. *J. Climate,* **7,** 81–105.

Jury, M. R., B. Pathack, and B. Parker, 1999: Climatic determinants and statistical prediction of tropical cyclone days in the southwest Indian Ocean. *J. Climate,* **12,** 1738–1746.

Kalnay, E., and Coauthors, 1996: NCEP/NCAR 40-Year Reanalysis Project. *Bull. Amer. Meteor. Soc.,* **77,** 437–471.

Kawamura, R., T. Matsumura, and S. Iizuka, 2001: Role of equatorially asymmetric sea surface temperature anomalies in the Indian Ocean in the Asian summer monsoon and El Nino-Southern Oscillation coupling. *J. Geophys. Res.,* **106,** 4681–4693.

Klein, S. A., B. J. Soden, and N.-C. Lau, 1999: Remote sea surface temperature variations during ENSO: Evidence for a tropical atmospheric bridge. *J. Climate,* **12,** 917–932.

Krishnakumar, K., B. Rajagopalan, and M. A. Cane, 1999: On the weakening relationship between the Indian monsoon and ENSO. *Science,* **284,** 2156–2159.

Krishnamurthy, V., and J. Shukla, 2000: Intraseasonal and interannual variability of rainfall over India. *J. Climate,* **13,** 4366–4377.

Krishnamurti, T. N., 1987: Monsoon models. *Monsoons*, J. S. Fein and P. L. Stephens, Eds., John Wiley and Sons, 467–522.

Lau, N. C., and M. J. Nath, 2000: Impact of ENSO on the variability of the Asian–Australian monsoons as simulated in GCM experiments. *J. Climate,* **13,** 4287–4309.

Lin, S. J., and R. B. Rood, 1996: Multidimensional flux from Lagrangian transport. *Mon. Wea. Rev.,* **124,** 2046–2086.

Liu, Q., X. Jiang, S.-P. Xie, and W. T. Liu, 2004: A gap in the Indo-Pacific warm pool over the South China Sea in boreal winter: Seasonal development and interannual variability. *J. Geophys. Res.,* **109,** C07012 doi:10.1029/2003JC002179.

Matsuno, T., 1966: Quasi-geostrophic motions in the equatorial area. *J. Meteor. Soc. Japan,* **44,** 25–43

Mlawer, E. J., S. J. Taubman, P. D. Brown, K. J. Iacono, and S. A. Clough, 1997: Radiative transfer for inhomogeneous atmosphere: RRTM, a validated correlated-k model for the longwave. *J. Geophys. Res.,* **102,** 16 663–16 682.

Morcrette, J. J., S. A. Clough, E. J. Mlawer, and M. J. Iacono, 1998: Impact of a validated radiative transfer scheme,

RRTM, on the ECMWF model climate and 10-day forecasts. Tech. Memo. 252, ECMWF, 47 pp.

Murtugudde, R., and A. J. Busalacchi, 1999: Interannual variability of the dynamics and thermodynamics of the tropical Indian Ocean. *J. Climate,* **12,** 2300–2326.

Nigam, S., and H.-S. Shen, 1993: Structure of oceanic and atmospheric low-frequency variability over the tropical Pacific and Indian Oceans. Part I: COADS observations. *J. Climate,* **6,** 657–676.

Reynolds, R. W., and T. M. Smith, 1994: Improved global sea surface temperature analyses using optimal interpolation. *J. Climate,* **7,** 929–948.

Roeckner, E., and Coauthors, 1996: Atmospheric General Circulation Model ECHAM4: Model description and simulation of present-day climate. Rep. 218, 82 pp. [Available from Max-Planck-Institut fur Meteorlogie, Bundesstr, 55, D-20146, Hamburg, Germany.]

——, and Coauthors, 2003: Atmospheric General Circulation Model ECHAM5: Part I. Rep. 349, 140 pp. [Available from Max-Planck-Institut fur Meteorlogie, Bundesstr, 55, D-20146, Hamburg, Germany.]

Schulz, J. P., L. Dumenil, and J. Polcher, 2001: On the land surface–atmosphere coupling and its impact in a single-column atmospheric model. *J. Appl. Meteor.,* **40,** 642–663.

Shukla, J., 1998: Predictability in the midst of chaos: A scientific basis for climate forecasting. *Science,* **282,** 728–731.

Soman, M. K., and K. Krishnakumar, 1993: Space–time evolution of meteorological features associated with the onset of the Indian summer monsoon. *Mon. Wea. Rev.,* **121,** 1177–1194.

——, and J. M. Slingo, 1997: Sensitivity of the Asian summer monsoon to aspects of sea-surface-temperature anomalies in the tropical Pacific. *Quart. J. Roy. Meteor. Soc.,* **123,** 309–336.

Sperber, K. R., and T. N. Palmer, 1996: Interannual tropical rainfall variability in general circulation model simulations associated with the Atmospheric Model Intercomparison Project. *J. Climate,* **9,** 2727–2750.

——, J. M. Slingo, and H. Annamalai, 2000: Predictability and relationship between subseasonal and interannual variability during the Asian summer monsoon. *Quart. J. Roy. Meteor. Soc.,* **126,** 2545–2574.

Su, H., J. D. Neelin, and C. Chou, 2001: Tropical teleconnection and local response to SST anomalies during the 1997–98 El Niño. *J. Geophys. Res.,* **106,** 20 025–20 043.

Tiedtke, M., 1989: A comprehensive mass flux scheme for cumulus parameterization in large-scale models. *Mon. Wea. Rev.,* **117,** 1779–1800.

Tompkins, A., 2002: A prognostic parameterization for the subgrid-scale variability of water vapor and clouds in a large-scale model and its use to diagnose cloud cover. *J. Atmos. Sci.,* **59,** 1917–1942.

Wang, B., R. Wu, and X. Fu, 2000: Pacific–East Asian teleconnection: How does ENSO affect East Asian climate? *J. Climate,* **13,** 1517–1536.

Watanabe, M., and F.-F. Jin, 2003: A moist linear baroclinic model: Coupled dynamical–convective response to El Niño. *J. Climate,* **16,** 1121–1139.

Wolter, K., and M. S. Timlin, 1998: Measuring the strength of ENSO—How does 1997/98 rank? *Weather,* **53,** 315–324.

Wu, R., and B. Kirtman, 2004: Impacts of the Indian Ocean on the Indian summer monsoon–ENSO relationship. *J. Climate,* **17,** 3037–3054.

Xie, P., and P. Arkin, 1996: Analyses of global monthly precipitation using gauge observations, satellite estimates, and numerical model predictions. *J. Climate,* **9,** 840–858.

Xie, S.-P., H. Annamalai, F. A. Schott, and J. P. McCreary, 2002: Structure and mechanisms of south Indian Ocean climate variability. *J. Climate,* **15,** 867–878.